actuators

MDPI

Article

Active Flow Control by Coanda Actuators for Aerodynamic Drag Reduction in a European-Type Truck

R. Bardera [1], J. C. Matías-García [1], E. Barroso-Barderas [1], J. Fernández-Antón [1] and A. A. Rodríguez-Sevillano [2,*]

[1] National Institute for Aerospace Technology (INTA), 28850 Madrid, Spain; barderar@inta.es (R.B.); matiasgjc@inta.es (J.C.M.-G.); barrosobe@inta.es (E.B.-B.); jferant@inta.es (J.F.-A.)
[2] Escuela de Ingeniería Aeronáutica y del Espacio, Universidad Politécnica de Madrid (UPM), 28040 Madrid, Spain
* Correspondence: angel.rodriguez.sevillano@upm.es

Abstract

Heavy vehicles present high aerodynamic drag. This results in significant fuel consumption and, consequently, high emissions of harmful substances. This study examines the variation in aerodynamic drag in a European-type truck with different trailer configurations. Passive flow control by geometry modifications of the rear part of the trailer and active flow control using the Coanda effect were tested, with the aim of improving the aerodynamic efficiency of the vehicle. To achieve this, a modular structure of a 1:30 scaled truck was designed to enable different trailer configurations. Drag measurements were performed with a two-component external balance, and PIV tests were conducted to correlate the drag reduction with the aerodynamic changes behind the trailer. Passive control reduced drag by up to 5.7%, and active flow control reduced it by up to 12.6% compared to the unmodified base trailer. PIV flow visualization confirms that blowing effectively reduces the recirculation zone behind the trailer.

Keywords: aerodynamic drag; truck; active flow control; Coanda effect

check for updates

Academic Editors: Hui Tang, Xin Wen and Feng Ren

Received: 10 October 2025
Revised: 6 November 2025
Accepted: 11 November 2025
Published: 13 November 2025

Citation: Bardera, R.; Matías-García, J.C.; Barroso-Barderas, E.; Fernández-Antón, J.; Rodríguez-Sevillano, A.A. Active Flow Control by Coanda Actuators for Aerodynamic Drag Reduction in a European-Type Truck. *Actuators* **2025**, *14*, 556. https://doi.org/10.3390/act14110556

Copyright: © 2025 by the authors. Licensee MDPI, Basel, Switzerland. This article is an open access article distributed under the terms and conditions of the Creative Commons Attribution (CC BY) license (https://creativecommons.org/licenses/by/4.0/).

1. Introduction

Heavy vehicles are considered aerodynamically inefficient compared to other vehicles. This is because they are bluff bodies not optimized from an aerodynamic point of view. A truck traveling at 100 km/h consumes up to 52% of the fuel to overcome aerodynamic drag [1]. In contrast, a passenger car, under the same conditions, consumes approximately four times less fuel to the same effect. Therefore, any reduction in aerodynamic drag on heavy vehicles will result in considerable fuel savings [2].

The typical airflow trajectories around a truck are displayed in Figure 1 without any component to optimize its drag. There are four main areas that influence the aerodynamic performance of trucks [1]: cab design, the separation between the cab and the trailer, the gap under the trailer, and the rear part of the trailer. These areas generate low-pressure zones and massive flow detachments that increase the drag of the truck. The aerodynamic disturbances generated by them can be reduced using passive or active actuators [3]. While passive elements (skirts, deflectors, spoilers. . .) do not require external energy to work [4–6], active flow control devices use energy to automatically adjust and improve the truck's aerodynamics, such as active shock absorbers, mobile spoilers [7], or blowing air [8] to induce Coanda effect on certain surfaces. The Coanda effect is a physical phenomenon consisting of the tendency of a fluid to adhere to a curved surface [9,10]. This phenomenon

has been used primarily as a flow control technique to reduce the take-off and landing distance of aircraft. However, it could also be applied to reduce noise, to improve film cooling, or it could be applied in road vehicles in order to improve their aerodynamic performances [11–13]. The Coanda effect can be generated in both laminar and turbulent flows. For example, it has been tested for modifying circulation on wings by injecting air tangentially over a rounded trailing edge of a wing or flap to keep the flow attached, effectively moving the stagnation point and increasing lift [14]. Another example is to deflect the exhaust jet of an engine without the need for complex mechanical parts, improving maneuverability [15].

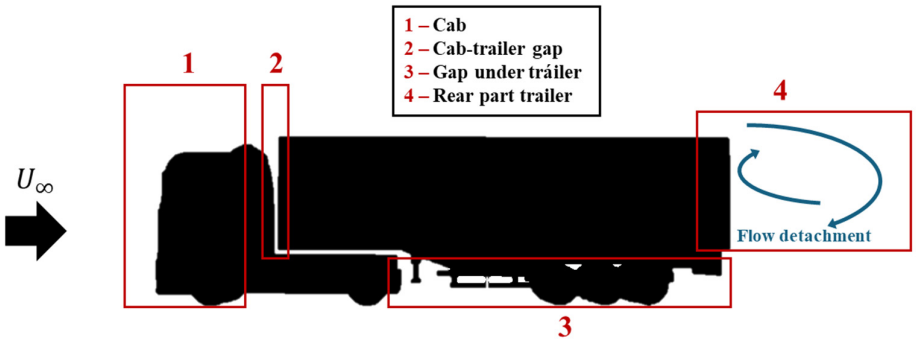


Figure 1. Critical areas that increase the aerodynamic drag of a truck.

In trucks, front deflectors, side skirts, and rear diffusers have been designed for reducing their aerodynamic drag. This results in important reductions in fuel consumption and CO2 emissions, making journeys more economical and sustainable. There are many projects oriented to reduce drag on heavy vehicles [16,17] (CONVENIENT, CO2RE, ECOCHAMPS, AEROFLEX, and FALCON), in which many solutions have been tested to improve the efficiency of heavy vehicles [1]. For example, Landman et al. [18] conducted wind tunnel tests with a full-scale heavy vehicle. They evaluated different configurations with passive elements, adding a lower front deflector, a front fairing with a lower deflector, a tapered rear fairing, and two different side skirts to a base truck. They achieved an important drag coefficient decrease of up to 28% with respect to the base case. Manosalvas et al. [19] developed a computational study implementing active flow control in a simplified geometric model of a heavy vehicle. They simulated the Coanda effect at the rear end of the geometric model, obtaining important reductions in aerodynamic drag as the jet pressure increased. They also concluded that as the radius of curvature increases, less energy is required in the jet for the proper working of this effect.

Improving aerodynamic efficiency not only reduces fuel consumption, but it also improves vehicle handling and reduces sensitivity to crosswinds, thereby increasing stability [20]. In this line, Chowdhury et al. [2] studied the influence of different external accessories on trucks under various yaw angles (0°, 5°, 10°, and 15°). They also tested a range of speeds from 40 km/h to 120 km/h, covering the gaps between vehicle parts, achieving a reduction in aerodynamic drag of up to 26%. A recent computational study performed by Phan [21] includes passive flow control devices on a 1:8 scaled truck. Side cabin extensions and rear spoilers with different deflection angles and lengths were tested. The optimal lengths and deflection angles of the side and rear extensions were determined with an important reduction of 20.8% in the drag coefficient. Cab roof fairings were investigated by Jae Kim et al. [22]. The results revealed aerodynamic drag reductions of 15% with a standard upper fairing, 16% including rounded edges of the fairing, and up to 18.6% optimizing the curvature and rounding the edges of the fairing.

Using the experimental facilities of the Experimental Aerodynamics Department of the National Institute of Aerospace Technology (INTA), the main goal of this paper is to

test different configurations of the rear part of a European truck trailer in order to reduce its aerodynamic drag. As displayed in Figure 2, geometry changes at the rear part of the trailer will be included as a passive flow control method. Active flow control by generating the Coanda effect at the same modified corner of the trailer will be analyzed to reduce the flow detachment behind the truck and then the aerodynamic drag. This Coanda effect is generated by injecting air on the curved corner of the trailer, in order to generate a low-pressure area and attract flow from the exterior of the boundary layer, in order to delay or eliminate the flow detachment. The aerodynamic drag coefficients of the truck will be presented for the different cases, as well as visualization with PIV behind the trailer to detect changes in the aerodynamic flow.

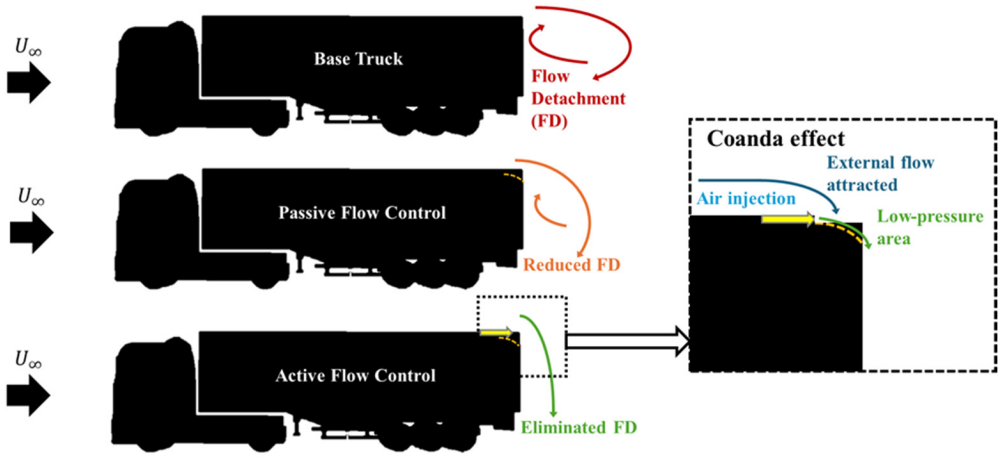


Figure 2. Comparison between the base truck aerodynamics and with Coanda effect generated.

The paper is structured in four sections. After the introduction, Section 2 describes the experimental set-up, including the base truck model and the trailers that were geometrically modified to introduce the Coanda effect. In the same section, the wind tunnels and external balance for force measurements are described. Finally, the experimental set-up used for visualization techniques with PIV (Particle Image Velocimetry) is presented. Section 3 presents the results of the aerodynamic drag for the different cases tested and the PIV velocity contours extracted. Section 4 includes the main conclusions of the paper.

2. Experimental Set-Up

2.1. Base Truck Model

The truck model is a European-type truck. It was printed using additive manufacturing in polylactic acid (PLA). The model has a removable rear section of the trailer so that the Coanda effect can be applied with different modules.

The model was scaled at 1:30. It had two parts: the cabin and the trailer. As displayed in Figure 3, overall dimensions were 552 mm × 82 mm × 132 mm. These dimensions meet three fundamental conditions. Firstly, the frontal area of the truck was 108.2 cm^2, which did not exceed 10% of the total area of the wind tunnel test chamber section to avoid a blockage condition. Truck length also left a margin of 10 cm between the nozzle and the diffuser of the wind tunnel in which force measurements were performed. To ensure flow similarity for blunt bodies such as trucks, a Reynolds number (*Re*) above 10^5 was required [23]. Once reached, the turbulent flow in the wake became similar, and aerodynamic characteristics did

not change with further increases in value. Taking the width of the truck as the characteristic length ($l_c = 82$ mm), a free-stream velocity $U_\infty = 15$ m/s, a $Re > 10^5$, calculated as,

$$Re = \frac{\rho U_\infty l_c}{\mu} \quad (1)$$

where ρ, and μ are air density and viscosity.

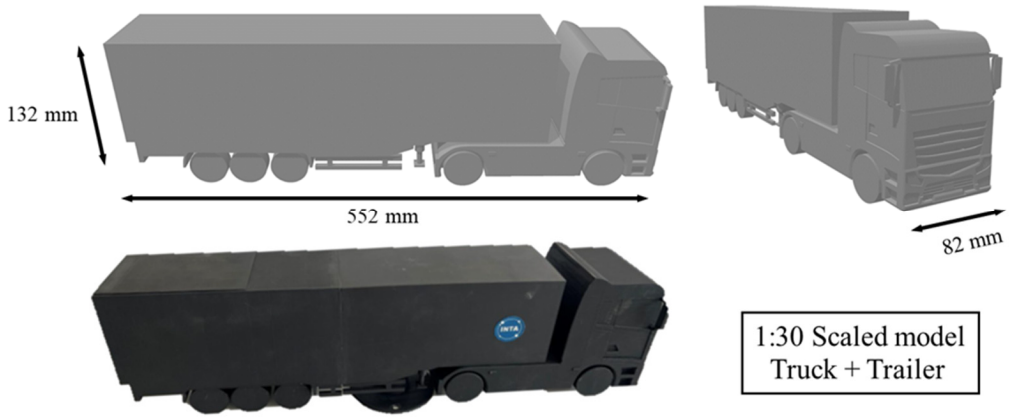


Figure 3. Model dimensions of the 1:30 truck and printed model for wind tunnel testing.

Finally, the aerodynamic drag force could not exceed the measurement range of the balance. With the 1:30 scaled model, and assuming a value of drag coefficient of $C_D \sim 1$, the expected force under 15 m/s would be around 1.5 N, this value is inside the range of measurement of the balance (9.8 N). The truck model at a scale of 1:30 met all the necessary conditions: it avoids blockage in the tunnel, it reaches the critical Reynolds number, and it generates a drag force inside the range of measure of the balance.

2.2. Trailers with Coanda Effect

The trailer was designed so that different modules could be attached to its rear part. This allowed for the testing of four different truck configurations: base, CS (superior curvature), CL (lateral curvature), and CSL (superior and lateral curvature). Except for the base model, the modules had a circular hole to allow air to enter, which generated the Coanda effect at the curved surfaces of the modules.

As displayed in Figure 4, the curved corners of the modules had a $b = 1.5$ mm slot to generate a tangential air jet on an arc of radius $R_C = 15$ mm. To introduce a jet on the modules to generate the Coanda effect, pressurized air was supplied into the modules of the trailer. A compressor ABC model XG-16 was used for this purpose. Finally, the outlet velocity of the slots where the Coanda effect pretends to be generated was measured using a hot-wire anemometer VelociCalic TSI 8345. Table 1 shows the different active flow control (AFC) cases of blowing tested (B1, B2, B3). The cases correspond to different air supplies with a flow control valve at the compressor outlet: B1 (almost closed), B2 (half-open), B3 (open). Then, there were three cases of blowing power: low (B1), medium (B2), and high (B3), resulting in the velocities (U_R) and mass flow rates ($\dot{m}$) measured at the outlet slot for the different modules (CS, CL, CSL). Note that the flow rate on each AFC case B1, B2, or B3 is practically the same, and outlet velocities increased as the slot outlet area was reduced.

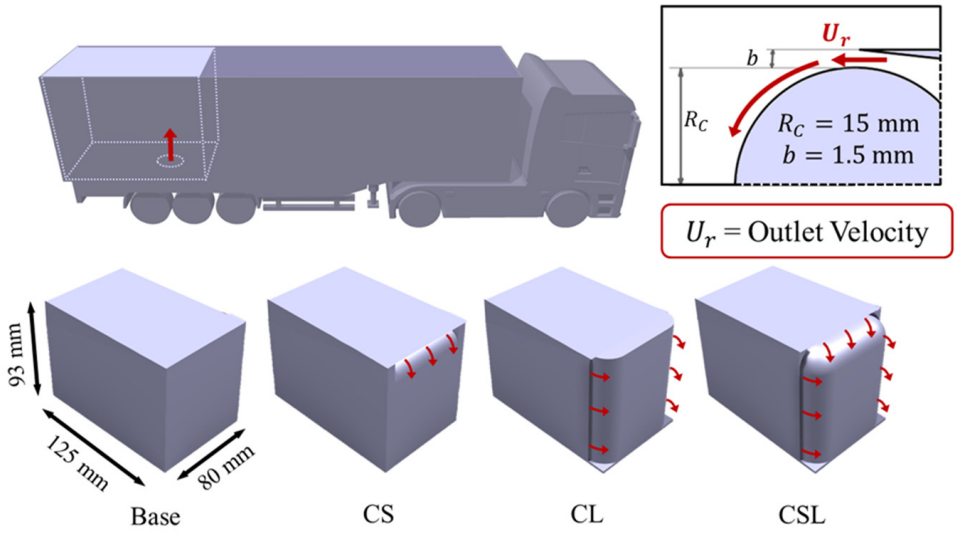


Figure 4. Three-dimensional modules manufactured: Base, CS, CL, CSL.

Table 1. Jet outlet velocities (U_r) in m/s and mass flow rate ($\dot{m}$) in kg/min for AFC generation.

AFC Case	B1		B2		B3	
Module	U_r	$\dot{m}$	U_r	$\dot{m}$	U_r	$\dot{m}$
CS	4.84	0.043 ± 0.010	9.92	0.126 ± 0.038	19.17	0.217 ± 0.056
CL	2.74		7.35		13.60	
CSL	1.27		5.33		7.91	

2.3. Force Measurements

In order to measure the aerodynamic drag of the truck with the different modules installed, a two-component external balance was used. The balance had two bending beam load cells with a measurement range of 1 kg. The load cells were joined at the ends as shown in Figure 5a.

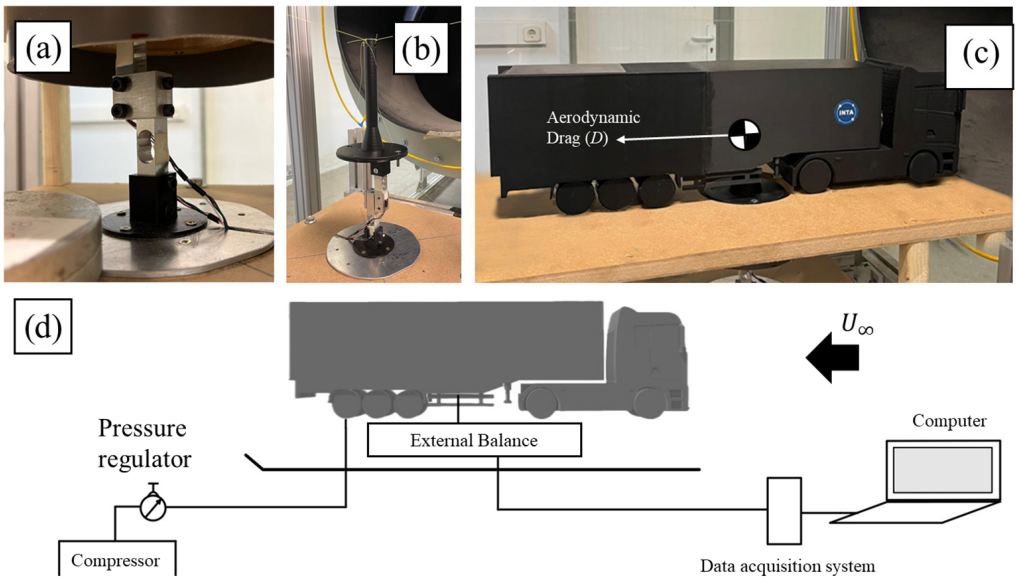


Figure 5. (**a**) External balance assembly. (**b**) Calibration body. (**c**) 1:30 truck model at the wind tunnel test section (**d**) Experimental set-up scheme for force measurements.

When a force is applied, the load cells undergo deformations, causing a change in the electrical signal, which is converted into forces by means of a calibration matrix. The calibration process was performed using a single-component and combined loads, applied with a calibration body specifically designed for this external balance (Figure 5b). After the calibration process, it was concluded that the error of the adjustment using linear, quadratic, and cross terms is less than 1.6% for the lateral component and 1.2% for the drag component. Moreover, during the verification process, the balance's measurement errors were less than 3.1%. Figure 5c displays the truck positioned in the Wind-Tunnel test section for aerodynamic drag determination. To simulate the ground, a complete wooden table covered the underside of the truck, and its front edge was rounded to avoid flow disturbances over its surface. For the active flow control tests, the full experimental set-up is shown in Figure 5d, in which the air supply required for generating the Coanda effect was adjusted with a pressure regulator, and the external balance signals are registered by a computer using a commercial data acquisition system (Hottinger Brüel & Kjaer (HBM) model MX840, Darmstadt, Germany).

2.4. Wind Tunnels

The tests were performed in two Wind Tunnels located at the Experimental Aerodynamics Department of the National Institute of Aerospace Technology (INTA), Spain. Force measurements were carried out in a commercial Westenberg Engineering's WK 860060-E wind tunnel (Figure 6a). It was an open wind tunnel with a closed test chamber of test section dimensions of 508 mm × 750 mm × 1200 mm. It had a 35 kW engine that moved a centrifugal axial fan that allowed performing tests of up to 60 m/s. It also had two anti-turbulence screens to ensure a turbulence level below 0.5%

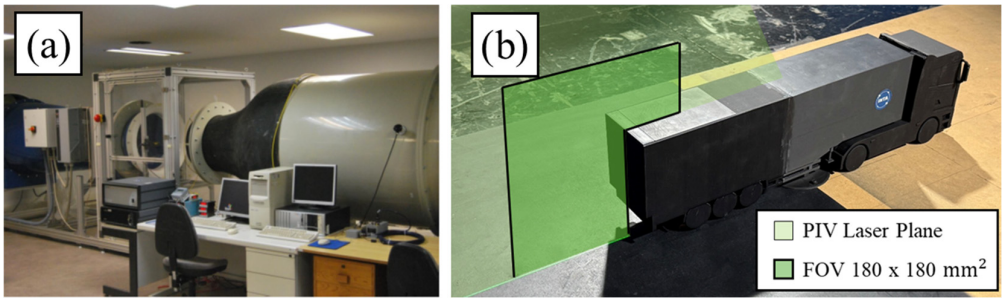


Figure 6. (**a**) WK 860060E Wind Tunnel. (**b**) PIV field of view.

Particle image velocimetry (PIV) [24–27] was used to obtain the flow visualization with velocity contours around the model. For the proper working of the PIV, small tracer particles of ~1 µm in diameter were seeded in the flow and illuminated using two neodymium-doped yttrium aluminum garnet Nd:YAG pulsed lasers. Synchronizing the laser pulses with the capture of pairs of photographs, the position of the particles were recorded with a digital camera and a 2048 × 2048 pixels charged coupled device (CCD) sensor. And as the time between the first and second image of the pair was known (Δt = 25 us), a cross-correlation process that used a Fast Fourier Transform (FFT) algorithm could determine the displacement of the particles and their velocity in small interrogation windows selected, at measurements of 32 × 32 pixels.

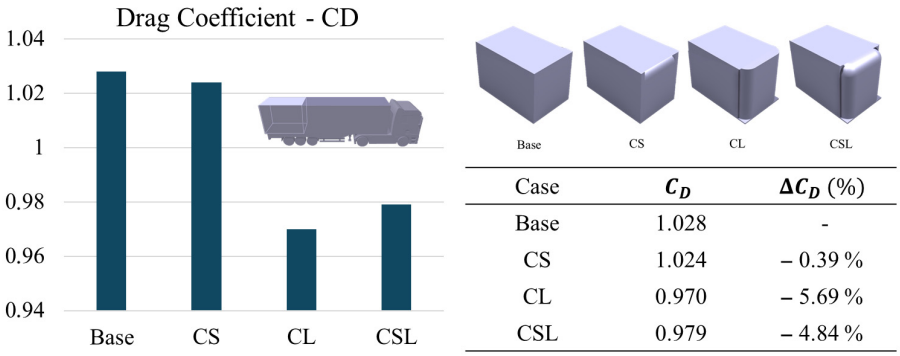
During the tests, the field of view for extracting velocity contours was 180 mm × 180 mm, right at the rear corner of the trailer (Figure 6b). All the velocity contours were obtained from 100 image pairs captured with a frequency rate of 1 Hz and represented in non-dimensional velocity contours using Tecplot360 2022 R1 software.

3. Results

3.1. Passive Flow Control

The tests with the four modules and without blowing results in the drag coefficients are displayed in Figure 7. The drag reductions in percentage are also displayed, calculated as,

$$\Delta C_D(\%) = \frac{C_{Di} - C_{Dbase}}{C_{Dbase}} \times 100 \quad (2)$$



Case	C_D	ΔC_D (%)
Base	1.028	-
CS	1.024	– 0.39 %
CL	0.970	– 5.69 %
CSL	0.979	– 4.84 %

Figure 7. Drag coefficient for base and modules without active flow control.

The module with curvature on the lateral (CL) provides a significant reduction in drag of 5.69% over the base truck. The trailer with a curvature at the top and sides (CSL) also shows a significant improvement of 4.84% but the curvature at the top (CS) presents only a small improvement of 0.39%.

PIV results with base trailer and modules CS, CL, and CSL without blowing are displayed in Figure 8. Base flow behind the trailer shows a low-speed zone dominated by several flow recirculations. Specifically, a recirculation zone can be observed close to the rear surface of the truck, and another one higher up, near the shear-layer region (in green) that limits the undisturbed flow above and the low-speed zone below. When the module with superior curvature (CS) is installed, the shear-layer becomes slightly wider at the beginning. However, the aerodynamic flow patterns behind the trailer remain unchanged. The module that adds lateral curvature (CL) or the one that combines the curved side and top corners (CSL) shows the same flow pattern again, although the streamlines seem to have lower intensity in the recirculation areas.

3.2. Active Flow Control: Coanda Effect

Figure 9 includes two plots: the drag coefficient for each case of active flow control (AFC), and drag reduction compared to each module without blowing.

The two graphics are plotted as a function of the non-dimensional velocity U_r^*,

$$U_r^* = U_r / U_\infty \quad (3)$$

where U_r is the velocity of the jet at the outlet to generate Coanda effect, and $U_\infty \sim 15$ m/s is the free-stream velocity.

The three tables included in Figure 9 display the numerical results of the drag coefficient for each module, and for the different cases of AFC tested: B1, B2, and B3. The percentage improvement compared to each of the models without blowing is also plotted and presented in the fourth column, calculated as,

$$\Delta C_D(\%) = \frac{C_{DxB_i} - C_{Dx}}{C_{Dx}} \times 100 \quad (4)$$

where C_{DxB_i} is the drag coefficient for each module ($x = CS, CL, CSL$) with active flow control applied (i =1, 2, 3), and C_{Dx} is the drag coefficient for each module without blowing.

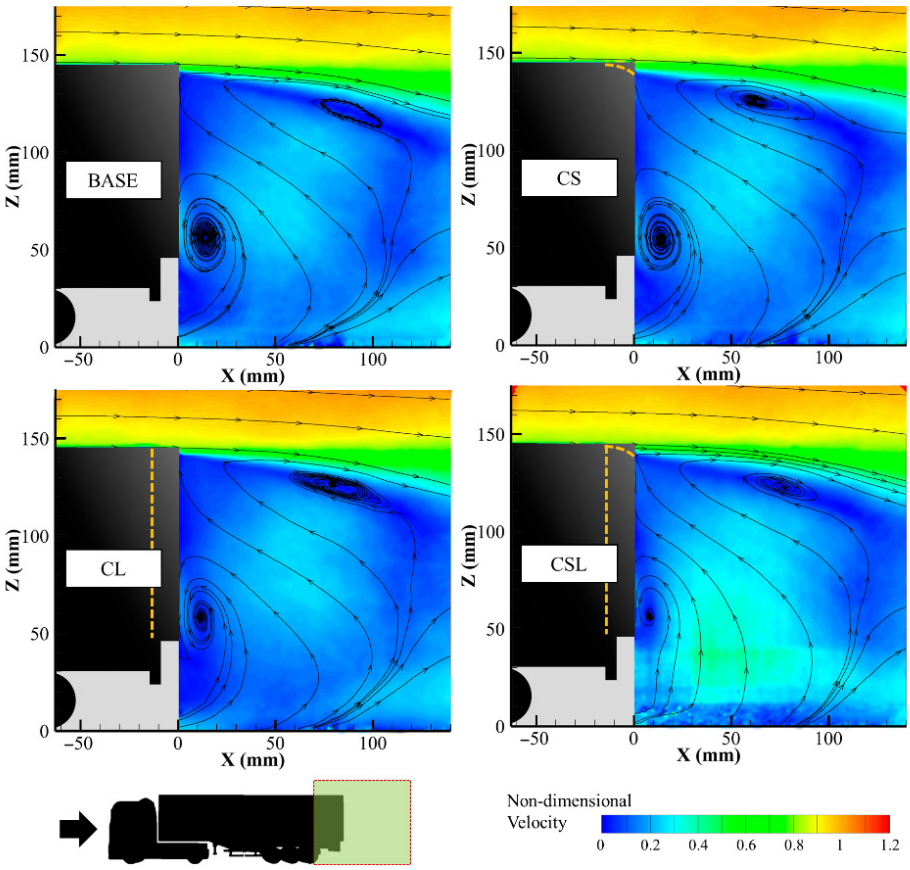
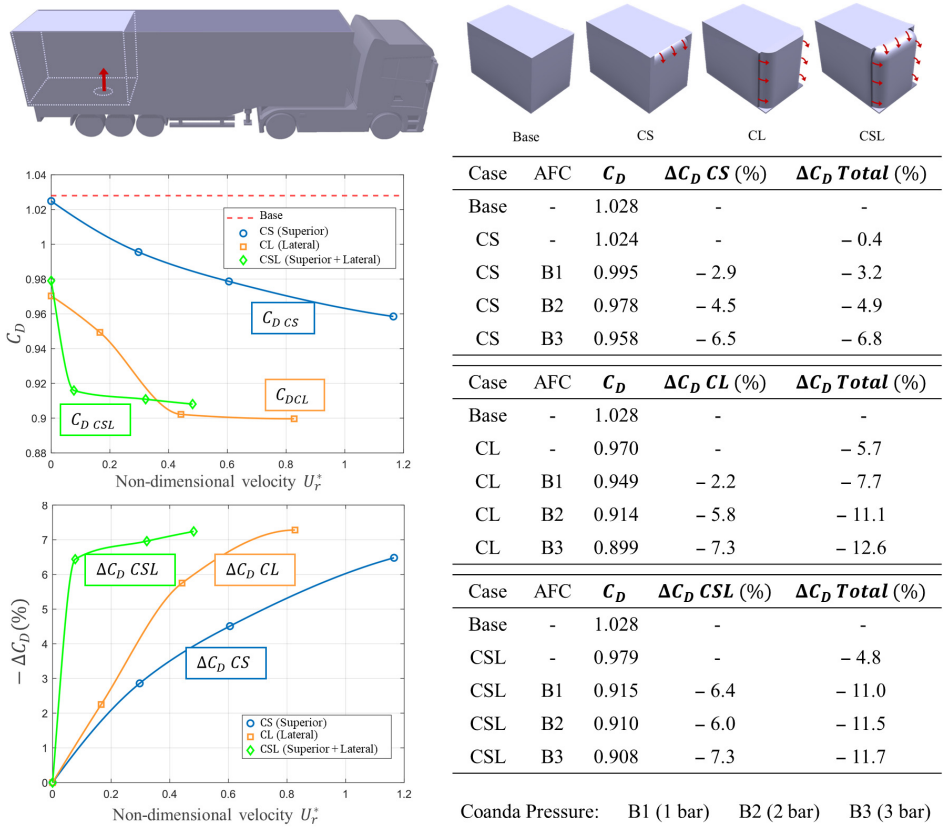


Figure 8. PIV results for base and modules without active flow control.



Case	AFC	C_D	ΔC_D CS (%)	ΔC_D Total (%)
Base	-	1.028	-	-
CS	-	1.024	-	– 0.4
CS	B1	0.995	– 2.9	– 3.2
CS	B2	0.978	– 4.5	– 4.9
CS	B3	0.958	– 6.5	– 6.8

Case	AFC	C_D	ΔC_D CL (%)	ΔC_D Total (%)
Base	-	1.028	-	-
CL	-	0.970	-	– 5.7
CL	B1	0.949	– 2.2	– 7.7
CL	B2	0.914	– 5.8	– 11.1
CL	B3	0.899	– 7.3	– 12.6

Case	AFC	C_D	ΔC_D CSL (%)	ΔC_D Total (%)
Base	-	1.028	-	-
CSL	-	0.979	-	– 4.8
CSL	B1	0.915	– 6.4	– 11.0
CSL	B2	0.910	– 6.0	– 11.5
CSL	B3	0.908	– 7.3	– 11.7

Coanda Pressure: B1 (1 bar) B2 (2 bar) B3 (3 bar)

Figure 9. Force coefficients for active flow control.

The drag coefficient is reduced as the power applied to the Coanda jet increases. CS shows a progressive decrease in the drag coefficient, but even at higher speeds of the Coanda jet, the drag coefficient does not fall below 0.95. The results for the trailer with lateral curvature (CL) and lateral and upper curvature (CSL) stand out above those for the trailer with upper curvature (CS), with coefficient values that reach 0.90.

Observing the reductions in the coefficient as a percentage compared to each module without blowing, CS module achieves reductions between 2.9 and 6.5%. The most significant improvements occur with the CL and CSL modules, achieving reductions of up to 7.3% compared to their respective case without blowing. It should be noted that the CSL module shows a significant improvement even for low outlet speeds (A). However, the lowest value of the drag is achieved for CL-B3 configuration.

The fifth column of tables in Figure 9 displays drag reduction with respect to the base trailer without any modification, calculated as,

$$\Delta C_D\ Total(\%) = \frac{C_{DxB_i} - C_{Dbase}}{C_{Dbase}} \times 100 \quad (5)$$

The resultant values of total drag reduction are represented also in Figure 10. It is clear that the CS module produces significant improvements over the base trailer, especially when blowing is applied. This result in overall drag reductions of between 0.4% and 6.8%. The case of CL and CSL is noteworthy because, without blowing, they already generate a significant reduction in resistance, of 5.7% and 4.8%, respectively. By applying AFC, the module that generates the lateral Coanda effect (CL) manages to reduce aerodynamic drag by between 7.7 and 12.6%. Finally, total drag is significantly reduced for the combined module (CSL), with very good reductions at low power of 11% (B1) and up to 11.7% at maximum power (B3). Thus, it could be said that although the best absolute results are obtained for the CL-C case, using the CSL module and the minimum blowing power (B1) already achieves a similar reduction in aerodynamic resistance, so this could be the optimal case: maximum drag reduction among the three minimum blowing power cases tested (B1).

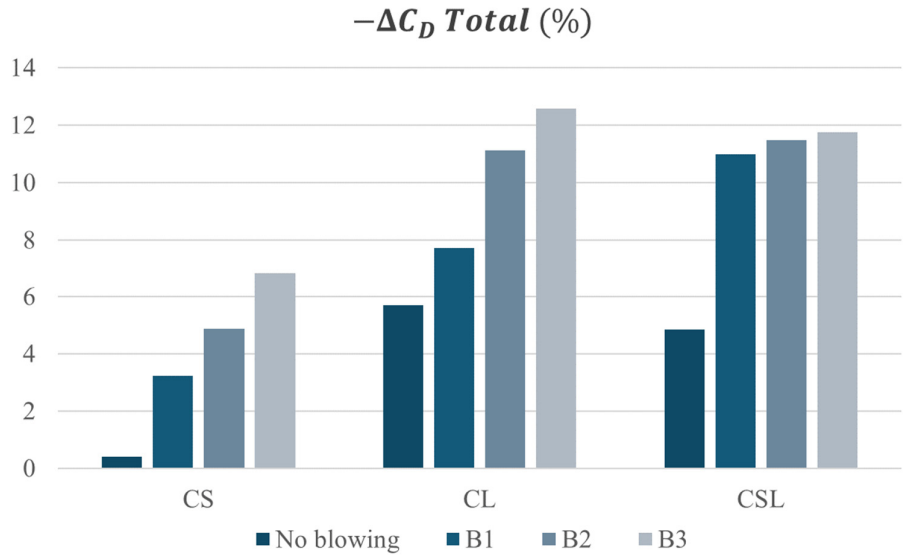


Figure 10. Total drag coefficient reduction for active flow control cases.

Finally, Figure 11 shows the dimensionless velocity contours obtained in all active flow control cases. This means that the results are shown for the CS, CL and CSL modules, with blowing activated B1, B2 and B3. In the case of lateral curvature (CL), adding blowing causes changes in the low-speed zone behind the truck. However, despite increasing the

blowing power, the recirculation zone is only slightly corrected in B3, as the recirculation stream-lines disappear, but the low-speed zone and the large separation produced at the rear corner of the trailer remain unchanged. In the case where blowing is applied at the upper corner (CS), the effects of active flow control are much more noticeable. With minimal blowing power (B1), the shear layer area is already modified, enclosing a large recirculation bubble but occupying much less area behind the truck. Even more remarkable is the reduction in the detached area in the CS-B2 case, where there is no longer a recirculation bubble behind the lorry, thanks to the blowing action.

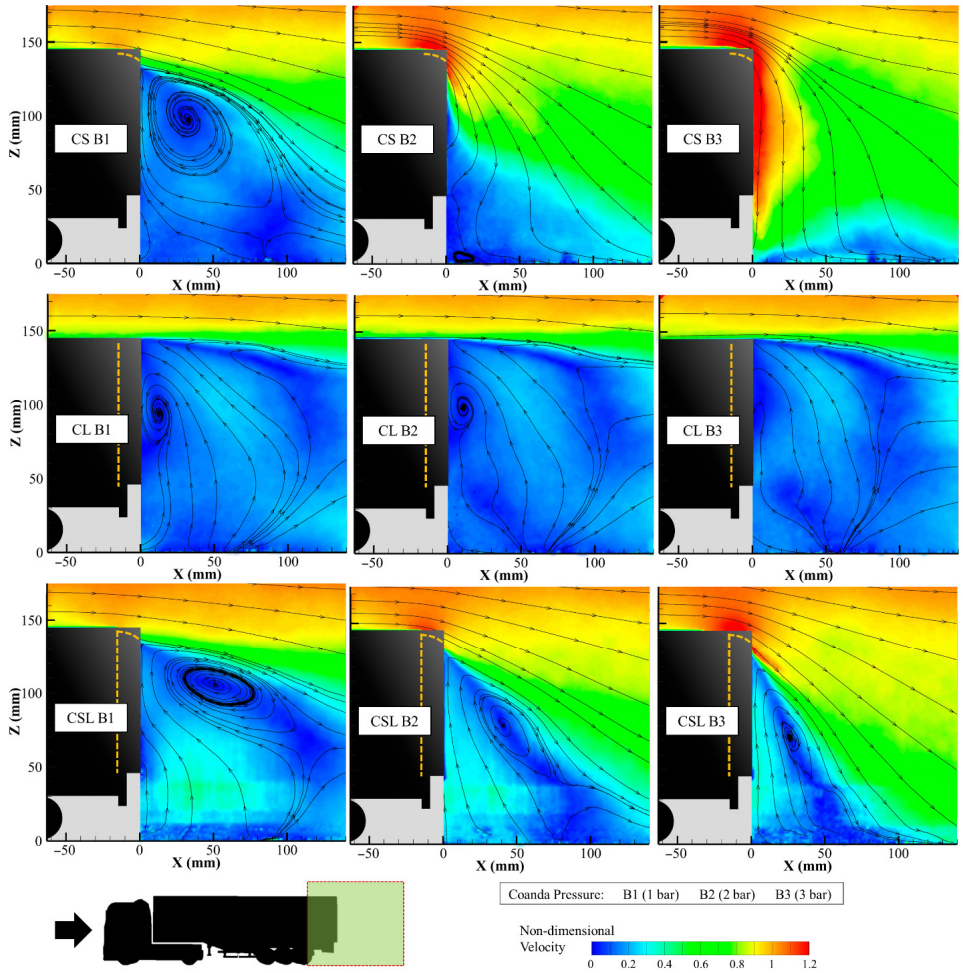


Figure 11. PIV results for CS, CL, and CSL active flow control.

However, the most striking effect is observed with the CS-B3 velocity contour, in which the blowing power is already enough to eliminate the low-speed zone behind the truck and the flow detachment produced at the rear corner. The active flow control manages to keep the flow attached to the rear part of the trailer, avoiding the undesirable effects of flow shedding, linked to increased aerodynamic drag.

Finally, combined blowing from the sides and top (CSL) also produces good results. Since more energy is applied to the blowing (B1, B2, and B3), the recirculation zone and low speeds are relegated to a smaller area behind the trailer, confirming that the Coanda effect appears in the designed geometry and maintains the flow attached, delaying or preventing flow separation. However, given that the velocity contour is taken on the central plane of the truck, there must be an interaction between the side and upper jets, which means that the detached flow is not completely eliminated, as is the case with the CS module.

The maximum reduction in flow separation is observed for case CS-B3. However, it should be noted that the flow behind the truck is highly three-dimensional, and therefore data from only the PIV on the central plane alone, may not capture all the flow patterns that affect its aerodynamic drag. For this reason, the PIV data are supplemented with smoke visualizations performed on the CS and CSL modules in Figures 12 and 13.

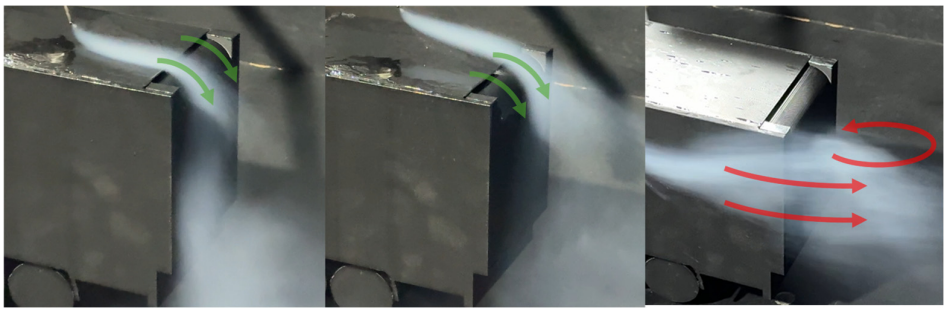


Figure 12. Smoke visualizations for the CS module with AFC.

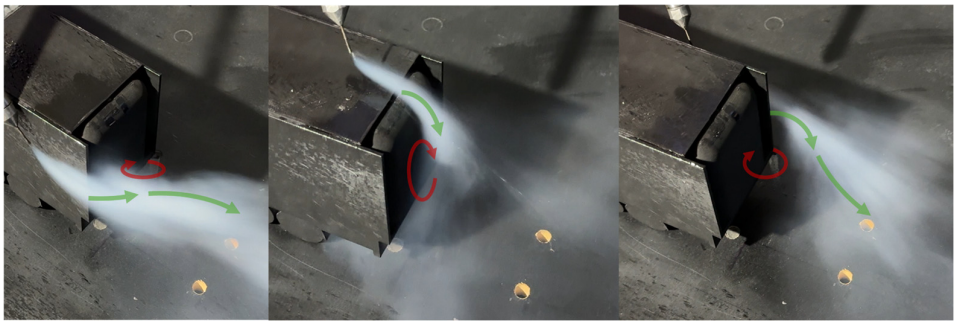


Figure 13. Smoke visualizations for the CSL module with AFC.

Specifically, Figure 12 shows that the Coanda effect generated by the CS module is maintained over the entire upper part (green arrows), but there are important flow detachments on the sides of the module (red arrows). However, in the visualization displayed in Figure 13, the CSL module has less flow adherence at the top that generates a small flow recirculation behind the trailer, but corrects flow detachment from the sides, resulting in a greater reduction in aerodynamic drag, as seen in the force measurements in the previous section.

4. Conclusions

In this paper, the reduction in the drag coefficient of a heavy vehicle with different trailer configurations by applying passive and active flow control has been analyzed. A base truck 1:30 scaled with a modular rear trailer was designed. Three different modules were tested and compared with the base truck: CS, CL, and CSL, depending on whether the curvature that generates the Coanda effect is on the top, sides, or both. To generate the Coanda effect, modifications were made to the corners, introducing circular arches that barely alter the shape of the truck, and adding small slots for pressurized air to escape.

From the results of the force measurements, the best performance without active flow control is for the CL module, with a reduction in the drag coefficient with respect to the base case of 5.7%. When the Coanda effect is applied, increasing jet power leads to a progressive reduction in the drag coefficient for all configurations. Specifically, the three configurations tested to improve their drag coefficient by between 2 and 7.3%, with respect to the non-blowing cases, and by between 3.2 and 12.6% with respect to the unmodified

trailer (base). Among all cases, the optimum drag coefficient with Coanda effect is the CSL-B1 module, since it provides maximum drag reduction with minimum blowing power.

Flow visualization with PIV confirms that blowing generates Coanda effect, which reduces the recirculation zone behind the trailer and helps the flow remain attached to the rear surfaces. As the air is injected from the slots, a low-pressure zone is created that attracts the flow outside the boundary layer, reducing the flow separation from the truck. This effect achieves a complete elimination of the recirculation region behind the truck for the CS-B3 module, and almost full elimination for the CSL-B2 and CSL-B3 modules. However, it is important to highlight the limitations of 2D PIV data obtained only on the central plane of the trailer. To register 3D flow patterns, flow visualizations with smoke were also presented, in which the CS module successfully maintained the Coanda effect along its entire upper surface, but significant flow detachments were still observed on the sides of the module. These flow detachments at the sides were effectively corrected by the CSL module, resulting in a greater overall reduction in the aerodynamic drag coefficient of up to 11.7%.

Active flow control applied to the rear of the truck trailer could be an effective way of reducing its aerodynamic drag. It only requires a small geometric modification to the rear corners of the trailer and the introduction of pressurized airflow through a small slot, achieving important reductions in aerodynamic drag coefficient and improving its aerodynamic wake by reducing flow separation and recirculation behind it. This could greatly improve the energy efficiency of future heavy vehicles as well as their stability and handling characteristics.

Author Contributions: Conceptualization, R.B. and A.A.R.-S.; Methodology, R.B., J.C.M.-G., E.B.-B., J.F.-A. and A.A.R.-S.; Validation, J.C.M.-G.; Investigation, J.C.M.-G., E.B.-B. and J.F.-A.; Data curation, J.C.M.-G.; Writing—original draft, J.C.M.-G.; Writing—review & editing, R.B., J.C.M.-G., E.B.-B. and J.F.-A.; Supervision, R.B. and A.A.R.-S.; Project administration, R.B. and A.A.R.-S. All authors have read and agreed to the published version of the manuscript.

Funding: This research was funded by Spanish Ministry of Defence.

Data Availability Statement: Dataset available on request from the authors.

Acknowledgments: The authors would like to thank the staff of the Experimental Aerodynamics department of INTA who participated in the tests presented in this paper. This study is included in the "Termofluidodinámica" program 464A 64 1999 14 205 0005 of the Spanish Ministry of Defense with INTA internal code IDATEC S.IGB21001.

Conflicts of Interest: The authors declare no conflict of interest.

References

1. Hariram, A.; Koch, T.; Mårdberg, B.; Kyncl, J. A study in options to improve aerodynamic profile of heavy-duty vehicles in Europe. *Sustainability* **2019**, *11*, 5519. [CrossRef]
2. Chowdhury, H.; Moria, H.; Ali, A.; Khan, I.; Alam, F.; Watkins, S. A study on aerodynamic drag of a semi-trailer truck. *Procedia Eng.* **2013**, *56*, 201–205. [CrossRef]
3. Choi, H. Control of flow over a bluff body. In Proceedings of the Fifth International Symposium on Turbulence and Shear Flow Phenomena, Munich, Germany, 27–29 August 2007; pp. 3–10. [CrossRef]
4. Cooper, K.R.; Leuschen, J. Model and full-scale wind tunnel tests of second-generation aerodynamic fuel saving devices for tractor-trailers. *SAE Tech. Pap. Ser.* **2005**, *1*, 3512. [CrossRef]
5. Gilliéron, P.; Kourta, A. Aerodynamic drag reduction by vertical splitter plates. *Exp. Fluids* **2009**, *48*, 1–16. [CrossRef]
6. Mohamed-Kassim, Z.; Filippone, A. Fuel savings on a heavy vehicle via aerodynamic drag reduction. *Transp. Res. Part D Transp. Environ.* **2010**, *15*, 275–284. [CrossRef]
7. Aider, J.-L.; Beaudoin, J.-F.; Wesfreid, J.E. Drag and lift reduction of a 3D bluff-body using active vortex generators. *Exp. Fluids* **2009**, *48*, 771–789. [CrossRef]

8. Littlewood, R.P.; Passmore, M.A. Aerodynamic drag reduction of a simplified squareback vehicle using steady blowing. *Exp. Fluids* **2012**, *53*, 519–529. [CrossRef]
9. Frunzulica, F.; Ionescu, T. Mathematical Modelling and Numerical Investigations on the Coanda Effect. In *Nonlinearity, Bifurcation and Chaos—Theory and Applications*; IntechOpen: London, UK, 2012; Chapter 5. [CrossRef]
10. Parks, E.; Petersen, R. Analysis of a "Coanda" type flow. *AIAA J.* **1968**, *6*, 4–7. [CrossRef]
11. Cerutti, J.J.; Sardu, C.; Cafiero, G.; Iuso, G. Active flow control on a square-back road vehicle. *Fluids* **2020**, *5*, 55. [CrossRef]
12. Barros, D.; Borée, J.; Noack, B.R.; Spohn, A.; Ruiz, T. Bluff body drag manipulation using pulsed jets and Coanda effect. *J. Fluid Mech.* **2016**, *805*, 422–459. [CrossRef]
13. Geropp, D.; Odenthal, H.-J. Drag reduction of motor vehicles by active flow control using the Coanda effect. *Exp. Fluids* **2000**, *28*, 74–85. [CrossRef]
14. Nishino, T.; Hahn, S.; Shariff, K. Large-eddy simulations of a turbulent Coanda jet on a circulation control airfoil. *Phys. Fluids* **2010**, *22*, 125105. [CrossRef]
15. El Halal, Y.; Marques, C.H.; Rocha, L.A.O.; Isoldi, L.A.; Lemos, R.d.L.; Fragassa, C.; dos Santos, E.D. Numerical Study of Turbulent Air and Water Flows in a Nozzle Based on the Coanda Effect. *J. Mar. Sci. Eng.* **2019**, *7*, 21. [CrossRef]
16. Connolly, M.G.; Ivankovic, A.; O'Rourke, M.J. Drag Reduction Technology and devices for road vehicles—A comprehensive review. *Heliyon* **2024**, *10*, e33757. [CrossRef] [PubMed]
17. Aultman, M.; Wang, Z.; Auza-Gutierrez, R.; Duan, L. Evaluation of CFD methodologies for prediction of flows around simplified and complex automotive models. *Comput. Fluids* **2022**, *236*, 105297. [CrossRef]
18. Landman, D.; Cragun, M.; McCormick, M.; Wood, R. Drag Reduction of a Modern Straight Truck. *SAE Int. J. Commer. Veh.* **2011**, *4*, 256–262. [CrossRef]
19. Manosalvas, D.E.; Economon, T.; Palacios, F.; Jameson, A. Techniques for the Design of Active Flow Control Systems in Heavy Vehicles. In Proceedings of the 33rd AIAA Applied Aerodynamics Conference AIAA Aviation, Dallas, TX, USA, 22–26 June 2015. [CrossRef]
20. Choi, H.; Lee, J.; Park, H. Aerodynamics of Heavy vehicles. *Annu. Rev. Fluid Mech.* **2014**, *46*, 441–468. [CrossRef]
21. Phan, T.L. Optimal configuration of passive flow control devices to reduce the aerodynamics drag of a tractor-trailer model. *Results Eng.* **2024**, *23*, 102425. [CrossRef]
22. Kim, J.J.; Lee, S.; Kim, M.; You, D.; Lee, S.L. Salient drag reduction of a heavy vehicle using modified cab-roof fairings. *J. Wind. Eng. Ind. Aerodyn.* **2017**, *164*, 138–151. [CrossRef]
23. Lim, H.C.; Castro, I.P.; Hoxey, R.P. Bluff bodies in deep turbulent boundary layers: Reynolds-number issues. *J. Fluid Mech.* **2007**, *571*, 97–118. [CrossRef]
24. Raffel, M.; Willert, C.E.; Scarano, F.; Kahler, C.J.; Wereley, S.T.; Kompenhans, J. *Particle Image Velocimetry: A Practical Guide*; Springer: Cham, Switzerland, 2018.
25. Adrian, R.J.; Westerweel, J. *Particle Image Velocimetry*; Cambridge University Press: Cambridge, UK, 2011.
26. Prasad, A.K. Particle image velocimetry. *Curr. Sci. Assoc.* **2000**, *79*, 51–60.
27. Adrian, R.J. Particle-imaging techniques for Experimental Fluid Mechanics. *Annu. Rev. Fluid Mech.* **1991**, *23*, 261–304. [CrossRef]

Disclaimer/Publisher's Note: The statements, opinions and data contained in all publications are solely those of the individual author(s) and contributor(s) and not of MDPI and/or the editor(s). MDPI and/or the editor(s) disclaim responsibility for any injury to people or property resulting from any ideas, methods, instructions or products referred to in the content.